STRUCTURAL MECHANICS OF LOBED INFLATABLE STRUCTURES

Andrew Lennon[1] **and Sergio Pellegrino**[2]

[1]*Consulting Engineer, The Old Laundry, Marlfield Village, Clonmel, Tipperary, Ireland, E-mail: andrew@innealtoir.org, Webpage: www.innealtoir.org*
[2]*Professor of Structural Engineering, Engineering Department, Cambridge University, Trumpington Street, Cambridge CB2 1PZ, England, E-mail: pellegrino@eng.am.ac.uk, Webpage: www.eng.cam.ac.uk/∼sp28*

ABSTRACT

Inflatable membrane structures have low mass and a small stowed volume. These characteristics make them attractive for numerous aerospace applications. Many configurations are possible for inflatable membrane structures and lobed configurations are amongst the most common. The structural behaviour of a lobed inflatable structure depends on the shape and size of the lobe. A configuration of particular interest is the lobed isotensoid. The isotensoid is a spheroidal shape that carries stress only in one direction under uniform internal pressure. Membrane structures with this configuration have applications as aerodynamic decelerators, in scientific ballooning, and as possible habitats for space and planetary exploration. Aspects of structural behaviour of interest to designers and analysts are the membrane stress, structural efficiency and structural stability.

Key words: Inflatable structures; lobed structures; tension structures; membranes; equilibrium; stability.

1. INTRODUCTION

Deployable structures form a class of structures with many applications. The common umbrella of Fig. 1 is probably the most familiar deployable structure. Space applications have been the most important driver in deployable structures technology and mature technologies are starting to appear [1, 2, 3]. Space launch vehicles have limited payload bays and spacecraft often require operational dimensions larger than the dimensions of the payload bays. The solution is to make the structures deployable, packing them for stowage in the payload bay and then deploying them after launch into space.

Membrane structures are a category of ultra-low-mass space structures that can be packaged very compactly. Spacecraft that have a small stowed volume and low mass can use launch vehicles that are small and inexpensive. Alternatively, they can be launched as one of a number of spacecraft on a larger launch vehicle to share costs. Recent work on membrane structures emphasises the growing importance of this branch of spacecraft engineering [4].

Figure 1. The umbrella, an example of a deployable structure

Membrane structures are a particular class of structures, comprised of thin films or foils which carry load primarily in tension. Membrane structures have a long history from animal skins to modern advanced spacecraft. Figs. 2 to 4 show soap bubbles, rubber balloons, and foil party balloons, which are commonplace examples of membrane structures.

Engineered membrane structures have a number of advantages for space applications, notably their low mass and their compact volume when stowed. Space structures that require large spatial dimensions are an attractive area for exploiting the characteristics of membrane structures. Examples of large, advanced membrane structures are reflectors such as the NASA Inflatable Antenna Experiment, solar sails, and aerodynamic decelerators for spacecraft [5, 6]. Figs. 5 to 7 show examples of engineered membrane structures for spacecraft applications.

Inflated membrane structures are structures where the membrane is deployed and held in place by internal pressure. Examples of advanced engineering membrane structures are the Inflatable Antenna Experiment, Mars Pathfinder gas-bag landing system, and proposed inflated telescopes, Figs. 8 and 9. Many membrane structures have lobes and the scientific balloon of Fig. 10 provides an example of a lobed inflatable membrane structure.

Figure 2. Soap bubble, an example membrane structure

Figure 3. Another example of a membrane structure, the rubber balloon

Figure 4. Foil party balloon, typically inflated with helium to make it float

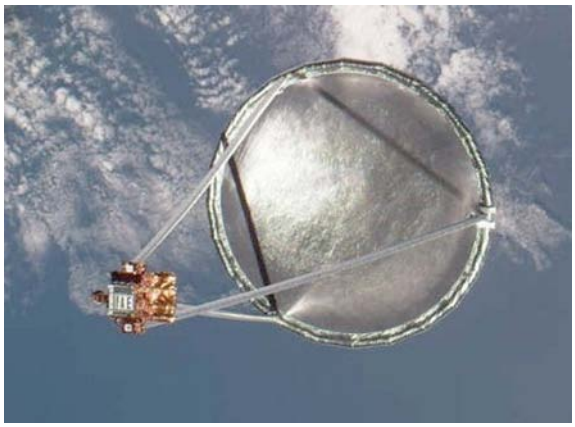

Figure 5. Inflatable antenna experiment (IAE)

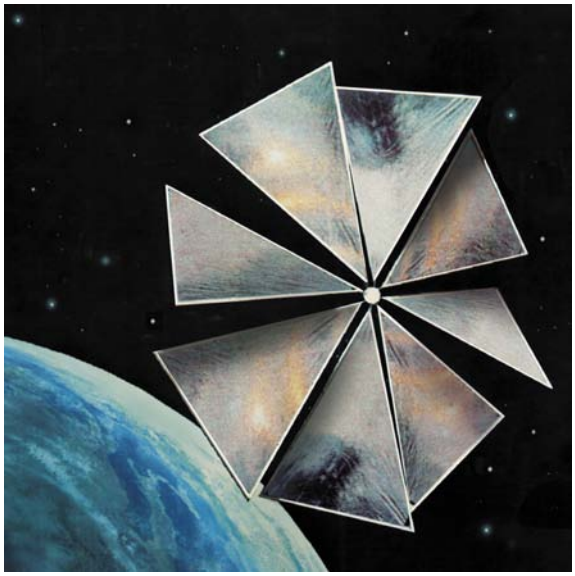

Figure 6. Artists concept of a solar sail (courtesy of Babakin Space Centre, The Planetary Society).

Figure 7. Parafoil to slow descent of experimental spacecraft

Figure 8. Inflated membrane structure — Mars Pathfinder landing gasbags (courtesy of NASA)

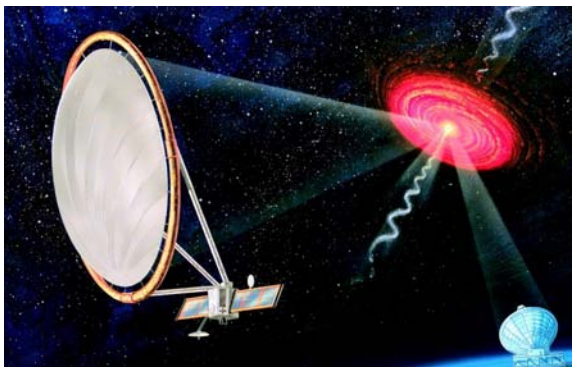

Figure 9. Inflated membrane structure — proposed ARISE telescope (courtesy of NASA)

Figure 10. Inflated membrane structure — NASA Long Duration Balloon (courtesy of NASA)

Using lobes simplifies manufacture and it allows the designer control over the distribution of stresses in the structure. The distribution of stresses in a lobed inflatable structure differs significantly from that in a non-lobed inflatable structure. Lobed structures can vary in their equilibrium configuration, maximum membrane stress, structural efficiency, and in their stability behaviour. Sects. 2 to 4 discuss some of the important relationships that govern the structural behaviour of lobed inflatable structures.

2. TENSION IN TWO-DIMENSIONAL LOBED MEMBRANE STRUCTURES

2.1. Overview

Membrane structures have negligible bending stiffness and can carry load only in tension. The forces acting on an inflated membrane structure are the pressure difference across the membrane and the tension in the membrane. A two-dimensional lobed structure provides a simple means of examining the equilibrium of lobed inflatable structures. The nodes at the intersection between adjoining lobes are set to a fixed distance from the centre of the structure.

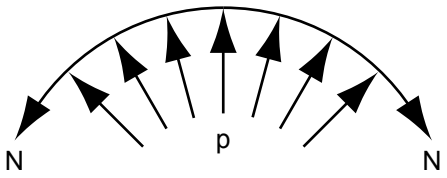

Figure 11. Equilibrium of two-dimensional curved membrane

Equilibrium of the membrane in Fig. 11 depends on the tension in the membrane N, the angle enclosed by

the membrane 2θ, and the pressure p across membrane. Equilibrium in the x-direction gives

$$2N\sin\theta = 2pr\sin\theta \tag{1}$$

$$N = pr \tag{2}$$

The tension is directly proportional to the radius of curvature of the membrane. One way to increase the curvature of the surface (i.e. decrease radius of curvature) is to use lobes. Lobes are highly-curved bulges on the structure. Comparing the lobed circle of Fig. 12 to the structure without lobes shows the effect of adding lobes on the membrane tension. The circle has a radius R and n identical lobes each of radius r each enclosing angle 2θ. The radial lines joining the centre of the circle to neighbouring lobe intersections subtends an angle 2ϕ as shown.

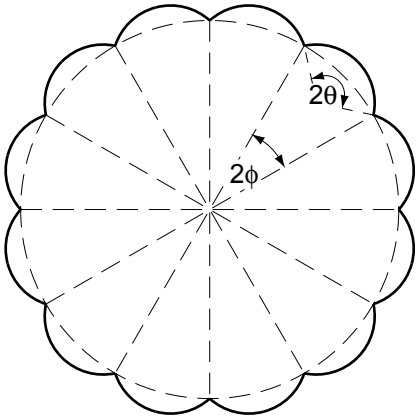

Figure 12. Equilibrium of a lobed circular membrane

The tension N_{lobe} in the lobe is

$$N_{lobe} = pr \tag{3}$$

2.2. Structural Efficiency

Replacing the lobed structure by a smooth circle of radius R gives membrane tension

$$N_{circle} = pR \tag{4}$$

The ratio between the membrane tensions is

$$\frac{N_{lobe}}{N_{circle}} = \frac{r}{R} \tag{5}$$

Now examine the circle of radius R_e that encloses the same area as the lobed configuration. The area A_e of this circle is

$$A_e = \pi {R_e}^2 \tag{6}$$

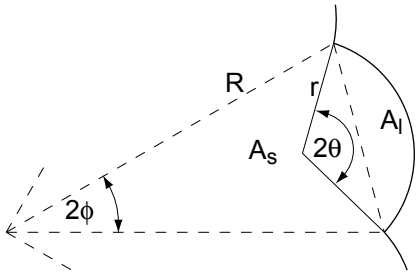

Figure 13. Area of lobed configuration

The area A_{total} of the lobed structure is the sum of the area of the lobes A_l and the sum of the areas A_s inside the lobes. Fig. 13 shows one segment of the lobed configuration.

$$A_{total} = n(A_l + A_s) \tag{7}$$

$$A_l = r^2\theta - r^2\sin\theta\cos\theta \tag{8}$$

$$A_s = R^2\sin\phi\cos\phi \tag{9}$$

Assembling these components gives

$$A_{total} = n\left(R^2\sin\phi\cos\phi + r^2\theta - r^2\sin\theta\cos\theta\right) \tag{10}$$

Note that $\phi = \frac{\pi}{n}$ and substitute to get

$$A_{total} = n\left(R^2\sin\left(\frac{\pi}{n}\right)\cos\left(\frac{\pi}{n}\right) + r^2\theta - r^2\sin\theta\cos\theta\right) \tag{11}$$

The radius of curvature of the lobe r depends on the radius R of the circle on which the lobes lie, the enclosed angle 2θ and the number of lobes n. The chord length across the lobe provides an expression linking these parameters.

$$r = \frac{R\sin\left(\frac{\pi}{n}\right)}{\sin\theta} \tag{12}$$

Substitute this expression for r into Eq. 11 to get

$$A_{total} = nR^2\,\sin\left(\frac{\pi}{n}\right)\cos\left(\frac{\pi}{n}\right) + nR^2\left(\frac{\sin\left(\frac{\pi}{n}\right)}{\sin\theta}\right)^2(\theta - \sin\theta\cos\theta) \tag{13}$$

Set areas calculated by Eqs. 6 and 13 to be equal to find the value of the radius R_e that has the same area as the lobed configuration.

$$R_e = \sqrt{\frac{A_{total}}{\pi}} \tag{14}$$

The value of R_e depends on the independent parameters R, n, and θ. The tension N_e in a membrane with this radius is

$$N_e = pR_e \tag{15}$$

The ratio between the tension in the lobed configuration and in the circular configuration that encloses an equal area is

$$\frac{N_{lobe}}{N_e} = \frac{r}{R_e} \tag{16}$$

Fig. 14 shows a plot of this ratio for a range of values of θ using $n = 16$.

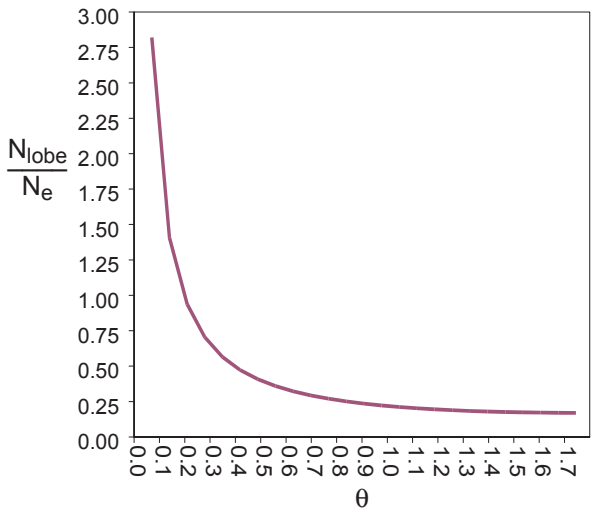

Figure 14. Ratio of the tensions in a lobed configuration and in the circle that encloses an equal area ($n = 16$)

Eq. 16 and Fig. 14 show the advantages of using lobes. A configuration with lobes has a lower tension than the circle that encloses the same area. Lower tension in the lobed configuration allows the use of a thinner membrane for the same stress, where stress σ is given by

$$\sigma = \frac{N}{t} \tag{17}$$

and t is the thickness of the membrane. If the maximum allowable stress is σ_{allow} then the minimum thickness of membrane t_{min} is

$$t_{min} = \frac{N}{\sigma_{allow}} \tag{18}$$

The mass m of membrane material is

$$m = \rho t s \tag{19}$$

where ρ is the density and s is the length.

The arc-length of a lobe is

$$s_{lobe} = 2r\theta \tag{20}$$

and the total length of the membrane for a lobed configuration is

$$s_{total} = 2nr\theta \tag{21}$$

Substitute for r from Eq. 12 to get

$$s_{total} = 2nR\theta \frac{\sin\left(\frac{\pi}{n}\right)}{\sin\theta} \tag{22}$$

The mass m_{total} of the lobed configuration is

$$m_{total} = \rho t_{lobed} s_{total} \tag{23}$$

Substitute from Eqs. 18 and 22 to get

$$m_{total} = \frac{2n\rho\ pR^2\theta}{\sigma_{allow}} \left(\frac{\sin\left(\frac{\pi}{n}\right)}{\sin\theta} \right)^2 \tag{24}$$

The equivalent expression for mass m_{circle} of a circular configuration of radius R is

$$m_{circle} = \frac{2\rho\, p\pi R^2}{\sigma_{allow}} \tag{25}$$

The ratio between the mass of the lobed configuration and the mass of the circular configuration is

$$\frac{m_{total}}{m_{circle}} = \frac{n\theta}{\pi} \left(\frac{\sin\left(\frac{\pi}{n}\right)}{\sin\theta} \right)^2 \tag{26}$$

This relationship can be expressed in terms of the ratio of the mass of the lobed configuration m_{total} to the mass of the circular configuration m_e that has the same enclosed area. Eq. 26 becomes

$$\frac{m_{total}}{m_e} = \frac{n\theta}{\pi}\left(\frac{R}{R_e}\right)^2\left(\frac{\sin\left(\frac{\pi}{n}\right)}{\sin\theta}\right)^2 \qquad (27)$$

Fig. 15 shows a plot of this ration for various values of θ using $n = 16$. This figure shows that the circular configuration requires less membrane material to enclose the same area for a given maximum stress. The length of the membrane for the lobed configuration is longer than for the circular configuration with the same enclosed area. The decrease in membrane thickness of the lobed configuration due to the lower tension is more than sufficient to counteract the effect of the increased length.

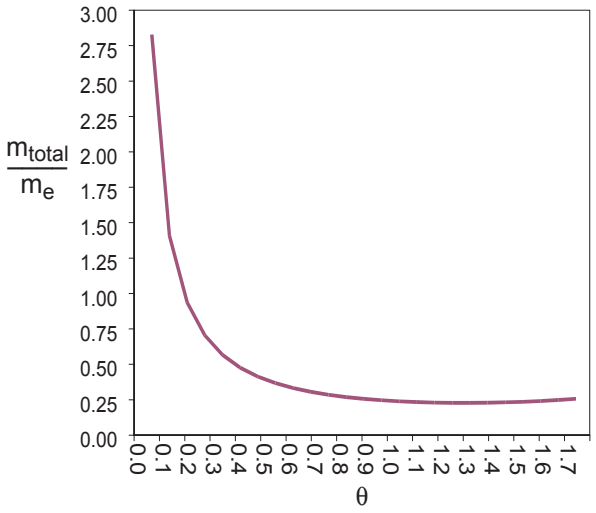

Figure 15. Ratio of the material requirement for lobed and circular configurations of equal area ($n = 16$

The relationships in Eqs. 5 to 27 assume that the lobes are identical. The lobes need not be identical and the equilibrium shape of the structure depends on the relative size of the lobes. Consider the two lobes of Fig. 16, which lie on a circle similar to that of Fig. 12.

Equilibrium in the x-direction gives

$$N_1 \sin\left(\frac{\pi}{2} + \phi_1 - \theta_1\right) = N_2 \sin\left(\frac{\pi}{2} + \phi_2 - \theta_2\right) \qquad (28)$$

Substitute from Eq. 3 and use the relationship from Eq. 12 to get

$$\left(\frac{\sin\phi_1}{\sin\theta_1}\right)(\cos(\phi_1 + \theta_1)) = \left(\frac{\sin\phi_2}{\sin\theta_2}\right)(\cos(\phi_2 + \theta_2)) \qquad (29)$$

This equation allows calculation of θ_1 and θ_2 for given values of ϕ_1 and ϕ_2.

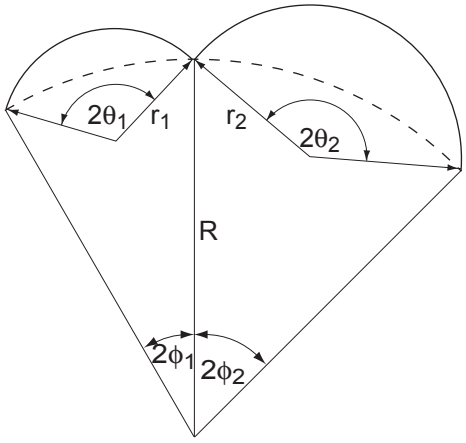

Figure 16. Two unequal sized lobes in an inflatable structure

2.3. Lobe Fullness

Lobe fullness is a measure of the amount of lobe material present for a given set of lobe parameters. Consider the lobes shown in Figs. 17 to 20. A lobe is under-full if the angle subtended by the lobes is less than that subtended by the radial lines at the edges of the lobe. In this case, the lobe has less curvature than the circle than the circle of radius R passing through the nodes joining the lobes. A lobe has 0% fullness if $r = R$ and it has 100% fullness (exactly-full) if the radial lines are tangential at the edges of the lobes. Eqs. 30, 31 and 32 provide the mathematical relationships describing under-full, partially-full, and exactly-full lobes.

$$\theta < \phi \qquad (30)$$
$$\theta > \phi \qquad (31)$$
$$\theta = \phi + \frac{\pi}{2} \qquad (32)$$

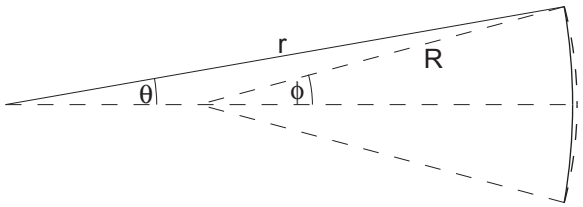

Figure 17. An under-full lobe

An over-full lobe is one with excessive material. The overfull lobe of Fig. 20 shows the edges of the lobe extending over the radial lines at the nodes of the lobe. Overfull lobes push against neighbouring lobes to give the shape in Fig. 21. The lobes now have two parts: a straight section at the intersection between neighbouring lobes, and a curved part that is exactly-full.

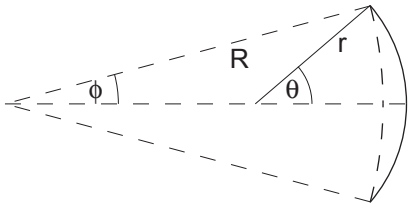

Figure 18. A partially-full lobe

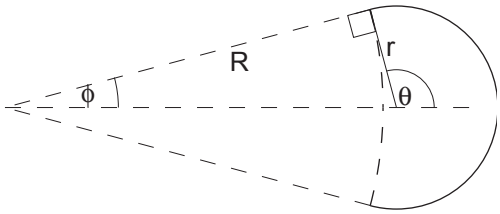

Figure 19. An exactly-full (100% full) lobe

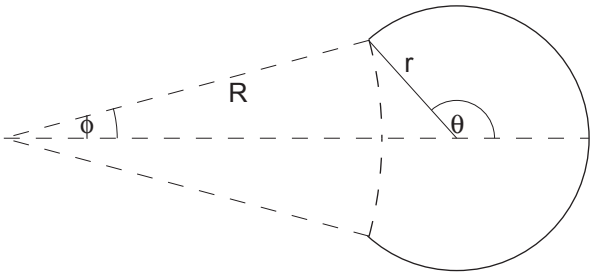

Figure 20. An over-full lobe

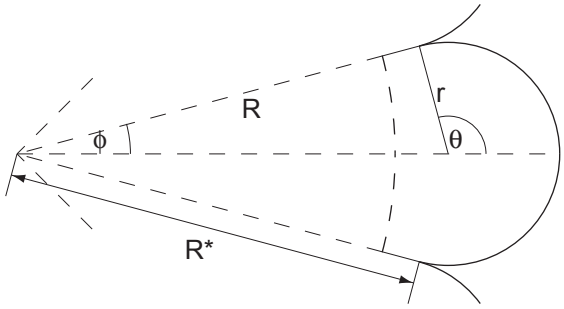

Figure 21. Realignment of an over-full lobe

The radius R can be replaced by the effective radius R^* as shown in Fig. 21. The value of R^* can be calculated by considering the length s of the material in the lobe, the radius R, and Eq. 32 to get

$$R^* = \frac{s + 2R}{2\,(1 + (\tan\phi)\,(\phi + \pi/2))} \tag{33}$$

The effective radius R^* is greater than the actual radius R for an overfull-lobe giving the condition for an overfull lobe.

$$s \geq 2R\,(\tan\phi)\,(\phi + \pi/2) \tag{34}$$

The tension in the lobe depends on the curved section of radius r and not on the straight section (see Eq. 1). Overfull lobes have a larger lobe radius than exactly-full lobes for the same values of ϕ and R. The over-full lobe has a higher membrane tension and uses a greater amount of membrane material than the equivalent exactly-full lobe making them structurally inefficient. The maximum stress reduction possible using lobes is for exactly-full lobes.

3. EQUILIBRIUM OF THREE-DIMENSIONAL MEMBRANE SURFACES

3.1. Overview

Sect. 2 deals with two-dimensional membranes and shows how the geometry of a membrane dictates the tension and structural efficiency of the structure. This section deals with three-dimensional membranes that resemble the behaviour of real structures.

3.2. Surface Equilibrium

Equilibrium of a membrane surface can be derived from shell theory by assuming that the bending stiffness is zero. Following Flügge, consider the equilibrium of a general infinitesimal element of membrane as shown in Fig. 22 [7]. The hoop edges of the element are defined by ϕ and $\phi + d\phi$, and the meridional edges are defined by θ and $\theta + d\theta$. The meridional and hoop tensions are denoted by N_ϕ and N_θ respectively, and the normal load is the pressure loading denoted by p.

An equation relating N_ϕ, N_θ and p can be found by examining equilibrium in the direction normal to the surface. The components to be considered are from the hoop tension, meridional tension and the distributed load. Write these components as

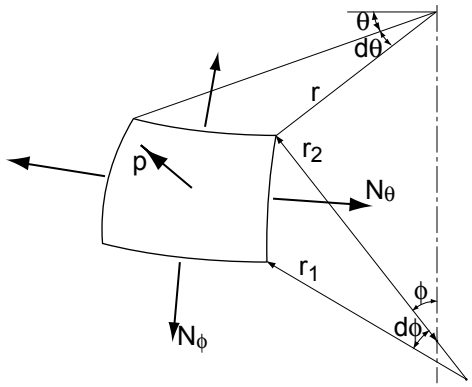

Figure 22. Surface element (after Flügge [7])

$$\text{hoop component} = N_\theta r_1 d\theta\, d\phi \sin\phi \quad (35)$$

$$\text{meridional component} = N_\phi r d\theta d\phi \quad (36)$$

$$\text{normal load component} = -prr_1 d\theta d\phi \quad (37)$$

Assembling these equations gives

$$N_\theta r_1 \sin\phi + N_\phi r - prr_1 = 0 \quad (38)$$

Radius r from this equation can be written as

$$r = r_2 \sin\phi \quad (39)$$

Divide by rr_1 and substitute for r from Eq. 39 to get

$$\frac{N_\phi}{r_1} + \frac{N_\theta}{r_2} = p \quad (40)$$

The simple example of a soap film or soap bubble subjected to uniform pressure p illustrates how Eq. 40 can provide useful information about the equilibrium surface. The membrane tension N is the same in all directions in a soap film or soap bubble [8]. Eq. 40 becomes

$$p = N\left(\frac{1}{r_1} + \frac{1}{r_2}\right) \quad (41)$$

Eq. 41 is the Laplace-Young equation. Define the mean surface curvature as

$$H = \frac{1}{2}\left(\frac{1}{r_1} + \frac{1}{r_2}\right) \quad (42)$$

If the $H = 0$ then $p = 0$ to satisfy Eq. 41. If $p = 0$ then the pressure is the same on each side of the membrane and the soap film does not form a bubble. To satisfy $H = 0$ either $r_1 = r_2 = \infty$ or $r_1 = -r_2$. The first case corresponds to a flat film that has zero curvature and the second case corresponds to a doubly curved anticlastic surface. A surface where $r_1, r_2 > 0$ and $r_1, r_2 \neq \infty$ requires $p > 0$. This surface is the familiar soap bubble.

3.3. The Isotensoid

The isotensoid is a special case of the doubly-curved surfaces of Section 3.2 that carries stress in only one direction. The isotensoid shape has a number of applications in the design and analysis of inflatable membrane structures. Fig. 23 shows a computer generated image of an isotensoid. Taylor derived the shape of the lobed isotensoid in a paper on the shape of parachutes [9]. This derivation assumes that the fabric of the parachutes transfer stress in the hoop direction to the meridional chords, which then transfer this load to the apex. The Taylor derivation also assumes that the fabric is taut in the hoop direction but on the point of wrinkling in the meridional direction. The resulting shape of the chords is a generator for the axisymmetric isotensoid. The parachute is a lobed isotensoid where isotensoid curves form the intersections between neighbouring lobes formed from parachute material.

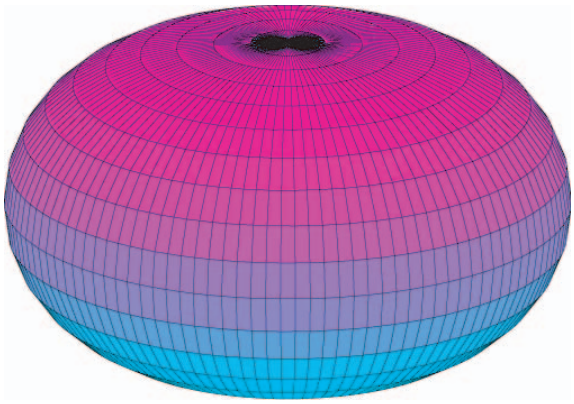

Figure 23. Isotensoid doubly-curved surface

The full derivation for the isotensoid surface starts with the shell equilibrium equations of Sect. 3.2. The hoop stress N_θ is zero for an isotensoid. The solution to the isotensoid equations involves the use of elliptic integrals and is beyond the scope of this discussion. Most work with isotensoids involves numerical solutions for the relevant calculations and a number of useful relationships can be established.

$$\frac{ds}{dr} = \frac{1}{(1 - \frac{r^4}{r_0^4})} \quad (43)$$

$$\frac{r^2}{r_0^2} = \sin\phi \quad (44)$$

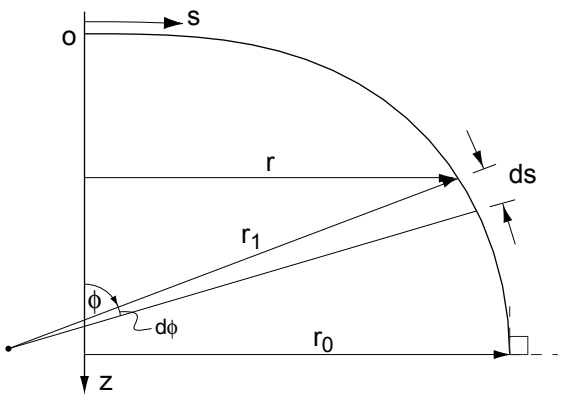

Figure 24. Vertical section through an isotensoid

where r_0 is the maximum horizontal distance from the central axis, Fig. 24.

The value of r_0 is related to the meridional length L_0 of the isotensoid by

$$r_0 = 0.381 L_0 \tag{45}$$

and to the maximum vertical height z_0 by

$$z_0 = 0.598 r_0 \tag{46}$$

Note that Eqs. 43 to 46 are independent of the value of the applied pressure. The relationship between distance along the meridional cord, s, and the horizontal ordinate, r, is uniquely determined for any value of r_0.

Kawaguchi investigated the shape of the shallowest possible axisymmetric pneumatic dome without wrinkles. The objective was to minimise the amount of unused space in a pneumatic dome subject to the constraint that the tangent to the dome had to be vertical at the base. Kawaguchi's study compared a hemisphere, a half ellipsoid, and a third shape that is shallower. For this shallowest shape the meridional tension N_ϕ and the hoop tension N_θ are

$$N_\phi = \frac{p r_2}{2} \tag{47}$$

$$N_\theta = p r_2 \left(1 - \frac{r_2}{2 r_1}\right) \tag{48}$$

If the structure is on the point of wrinkling then the hoop tension N_θ is zero and the radii of curvature are related by $r_1 = r_2/2$. Kawaguchi found that the cross-sectional area A_i is given by

$$A_i = r_0^2 \tag{49}$$

Eq. 49 can be verified using numerical calculations. For comparison, the area of a semi-circle is $A_c = \pi r^2/2$. For the case $r_0 = r$ the shallowest dome has a cross-sectional area 64% of that of the semi-circle. Numerical calculations also show that the distance of the centroid from the central axis r_c is given by

$$r_c = 0.436 r_0 \tag{50}$$

Kawaguchi's shallowest surface carries only meridional tension, therefore a cross-section is identical to the shape of the cords studied by Taylor [9]. Note that Eqs. 43 and 44 are scale independent hence the shape of the surface is unaffected by the meridional length. The surface shape is independent of the internal pressure and the magnitude of the membrane stress.

3.4. Structural Efficiency

The effect of using lobes in three-dimensional structures can be demonstrated by comparing an inflated sphere of radius r_s to a lobed isotensoid. Eq. 40 gives the membrane tension N_s as

$$N = \frac{p r_s}{2} \tag{51}$$

Note that the tension in a sphere is half that in a cylindrical surface. The lobed isotensoid can be constructed such that the lobes carry load only in the local hoop direction, with the membrane slack in the meridional direction. The lobes transfer the load to strong tapes or cords between the lobes that carry the load to the vertices. At the vertices a combination of load in the tapes and internal pressure keeps the structure in equilibrium. Setting the meridional tension $N_\phi = 0$ in Eq. 40 gives

$$N_\theta = p r_l \tag{52}$$

where r_l is the radius of curvature of the lobe in the hoop direction. Note that this relationship is the same as that for the two-dimensional lobe given by Eq. 2.

Comparing the tension in the smooth sphere to an isotensoid of n lobes shows that there is a considerable reduction in tension in the membrane. The tension in a lobe is $N_\theta = p r_l$ and the lobe meridional tensional is zero.

The lobe radius of curvature is typically much less than that of the sphere and adding lobes can significantly reduce the membrane stress. If the lobes carry load only in the hoop direction then the meridional tapes carry all of the meridional load. Designing inflatable structures in this way can increase the structural efficiency by facilitating optimisation of the load-carrying capacity of each structural member. Note that in Eq. 52 the value of N_θ varies with r_l therefore if the lobe radius of curvature is

constant then the tension in the membrane is constant. This relationship allows the structural designer to specify a constant radius of curvature for the lobes to give constant stress in the membrane.

Consider the case where the sphere has the same volume as the isotensoid without lobes. According to a theorem of Pappus if a plane figure rotates about an axis in its own plane then the volume generated is equal to the area of the figure multiplied by the distance travelled by the centroid of the figure [11, quoted in]. Use V_s to denote the volume of the sphere and V_i to denote the volume of the isotensoid. The volumes are

$$V_s = \frac{4}{3}\pi r_s^3 \quad (53)$$

$$V_i = 2\pi r_c A_i \quad (54)$$

where r_c is the centroid distance from Eq. 50 and A_i is the area enclosed between the curve and the central axis from Eq. 49.

Substituting expressions for r_c and A_i into Eq. 54 and equating to Eq. 53 gives

$$r_0 = 1.152\, r_s \quad (55)$$

Substitute r_l for r in Eq. 12 and substitute the resulting expression into Eq. 52 to get

$$N_\theta = p r_0 \frac{\sin\frac{\pi}{n}}{\sin\alpha} \quad (56)$$

Substituting for r_0 from Eq. 55

$$N_\theta = 1.152\, p r_s \frac{\sin\frac{\pi}{n}}{\sin\alpha} \quad (57)$$

Comparing with N from Eq. 51

$$\frac{N_\theta}{N} = 2.304\, \frac{\sin\frac{\pi}{n}}{\sin\alpha} \quad (58)$$

Note that the ratio between the stresses is independent of r_0 and r_l. The only geometric considerations are n and α thus the ratio is scale independent.

Fig. 25 shows plots of Eq. 58 for different numbers of lobes ($n = 32, 64, 128, 256$ and 512) with the tension ratio on the vertical axis and the lobe angle α on the horizontal axis. This ratio decreases with increasing number of lobes and with increasing lobe angle. This relationship provides a strong incentive for designers to use a large number of lobes and large lobe angles to decrease the membrane stress in inflatable structures.

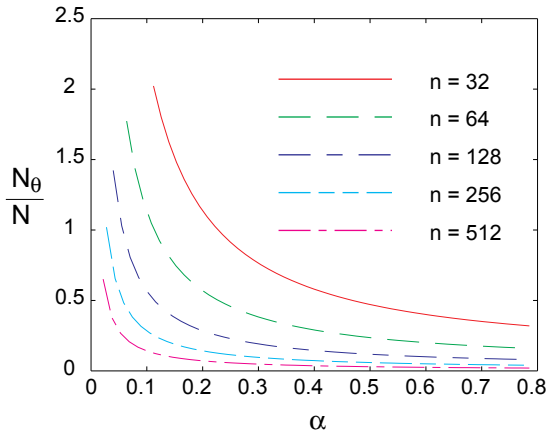

Figure 25. Ratios of stress in sphere and lobed isotensoids with different numbers of lobes

4. STABILITY

4.1. Overview

Stability is a problem that affects many classes of structure and lobed inflatable structures are one of these classes. Membranes can carry load only in tension and membrane structures exhibit unstable behaviour if compressive stresses occur. Lobed inflatable structures can also become globally unstable even if the membrane carries only tensile stress. This section briefly discusses the global instability of lobed membrane structures carrying tensile stress. Fig. 26 is a two-dimensional lobed column that demonstrates how these structures can become globally unstable. Structural stability can be assessed either by examining the potential energy of the structure or by examining the structural stiffness. Sect. 4.2 outlines how the lobed column of Fig. 26 can be assessed by examining the potential energy and Sect. 4.3 shows how stability can be assessed by equivalent stiffness methods.

4.2. Potential Energy Methods

A structure is stable if it has a local minimum of potential energy. The potential energy for an inextensible inflatable structure containing a fixed mass of gas at constant pressure and temperature depends only on the enclosed volume. A configuration is unstable if the structure can adopt another configuration that has greater enclosed volume.

Stability of the two-dimensional lobed column of Fig. 26 depends on the area that it encloses. Fig. 27 shows a deformed configuration for this column where the centreline forms an arc of a circle and each segment is identical in the deformed configuration. Assessing the stability of the column requires a comparison between the

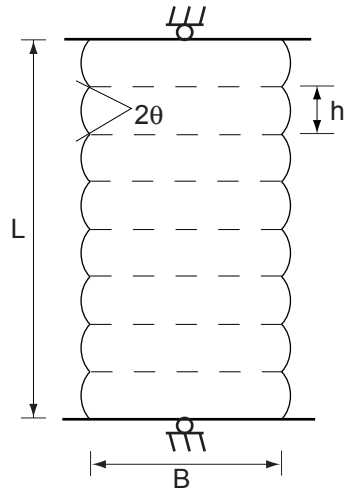

Figure 26. Lobed column (after Calladine [12])

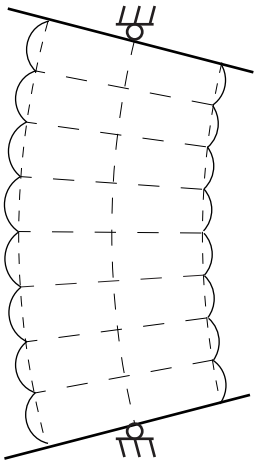

Figure 27. Deformed lobed column

enclosed areas of a segment for the deformed and undeformed configurations. The full derivation of the areas of each configuration is beyond the scope of this discussion but the final expression derived by Calladine can be reproduced [12].

$$6\left(\frac{Bh}{L^2}\right) \geq \frac{1}{A_l''} \tag{59}$$

where A_l'' is the second derivative of the area of a lobe with respect to the chord length.

$$A_l'' = -\frac{1}{2}\left(\frac{\cos\theta + \theta\,\sin\theta}{\sin\theta - \theta\,\cos\theta}\right) \tag{60}$$

4.3. Equivalent Stiffness Methods

Assessing the equivalent stiffness of the structure provides an alternative to examining the potential energy. The structure becomes unstable if the stiffness is negative, corresponding to negative eigenvalues in the stiffness matrix. It is not necessary to calculate the stiffness matrix here and a structural analogy can be used instead.

The end-cap pressure effect causes the lobed column to push against the pinned support at each end. This load is equivalent to a compressive load on a pinned strut. Axial deformation of the lobes causes a reaction that is proportional to the amount of deformation. Combining the load and deformation behaviour of the lobed column shows that its structural behaviour is equivalent to that of an elastic strut under compressive load, which is the Euler strut. Calladine's expression for EI, the stiffness for the two-dimensional column under pressure p can be used [12].

$$EI = -\frac{phB^2}{2}A_l'' \tag{61}$$

The condition for stability of an Euler strut is

$$F \leq EI\left(\frac{\pi}{L}\right)^2 \tag{62}$$

The end-cap effect of the pressure produces a load

$$F = pB \tag{63}$$

Combining Eqs. 61, 62, and 63 gives the condition for stability of the lobed column based on equivalent stiffness.

$$\left(\frac{\pi^2}{2}\right)\left(\frac{Bh}{L^2}\right) \geq \frac{1}{A_l''} \tag{64}$$

Eq. 59 has an initial factor of 6 rather than the factor of $\pi^2/2(= 4.935)$ of Eq. 64. This difference can be explained by the difference in the assumed deformed shapes. The potential energy methods assumes that the deformed centreline lies along an arc of a circle and the equivalent stiffness method assumes that the deformed centreline lies along a sine curve.

4.4. Extending The Methods

The lobed column of Fig. 26 is a simple example to demonstrate how the stability of lobed inflatable structures can be assessed and these methods can be extended to more complex structures in three-dimensions. Lennon and Pellegrino use the energy method to examine the stability of a three-dimensional lobed column and the lobed isotensoid [13]. Lennon proposes using structural analogies to determine the equivalent stiffness of lobed structures [14]. Pagitz et al. have developed computational methods for assessing the stability of inflatable membrane columns with extensible membranes [15].

5. DISCUSSION

Lobed inflatable structures have lower membrane tension than the equivalent unlobed structure. Using lobes also allows designers to choose a stress state that optimises the structural action of the various structural elements. The lobed isotensoid provides an example of a configuration where the lobes can be designed with constant curvature to carry constant uniaxial load in the hoop direction and to carry all meridional load via load-carrying tapes that run between the vertices. Lobed structures also have the advantage that the reduction in membrane thickness more than offsets the increase in surface area for a given value of allowable stress.

Structural instability is not a problem normally associated with structures that carry load entirely by tension but it can occur for lobed inflatable structures. The structural behaviour of the lobes is similar to that of an elastic structure and the action of the internal pressure on the structure causes a system of forces that behave in a similar manner to external compressive forces on a stiff structure. Combining the force behaviour and virtual elasticity causes the lobed structures to have stability problems analogous to stiff structures such as struts or shells. The stability of the lobed structures can be assessed by using potential energy calculations or by effective stiffness calculations.

REFERENCES

1. Gantes, C.J., *Deployable Structures: Analysis and Design*, WIT Press, Southampton, 2001.

2. Mollerup, P., *Collapsibles*, Thames and Hudson Ltd., London, 2001.

3. Beukers, A. and van Hinte, E., *Lightness*, 010 Publishers, Rotterdam, 2001.

4. Jenkins, C.H.M. (ed.), *Gossamer Spacecraft: Membrane and Inflatable Structures Technology for Space Applications*, AIAA, Reston, VA, 2001.

5. Freeland, R.E. and Veal, G.R., Significance of the Inflatable Antenna Experiment Technology, *39th AIAA/ASME/ASCE/AHS/ASC Structures, Structural Dynamics, and Materials Conference and Exhibit*, Long Beach, CA, 20–23 April, 1998.

6. McInnes, C.R., *Solar Sailing: Technology, Dynamics and Mission Applications*, Springer-Praxis, London/Chichester, 1999.

7. Flügge, W., *Stresses in Shells*, Springer Verlag, New York, NY, 1967.

8. Isenberg, C., *The Science of Soap Films and Soap Bubbles*, Dover, New York, NY, 1992.

9. Taylor, G.I., On the Shapes of Parachutes (Paper written for the Advisory Committee on Aeronautics, 1919), in *The Scientific Papers of G.I. Taylor*, Vol. 3, 26–37, Batchelor, G.K. (ed.), Cambridge University Press, Cambridge, 1963.

10. Kawaguchi, M., The Shallowest Possible Pneumatic Forms, *Bulletin of the IASS*, Vol. 18, 3–11, 1977.

11. Stroud, K.A., *Advanced Engineering Mathematics*, Macmillan Press Ltd., Basingstoke, 1995.

12. Calladine, C.R., Stability of the Endeavour Balloon, *Buckling of Structures*, 133–149, Elishakoff et al (ed.), Elsevier Science Publishers, Amsterdam, 1988.

13. Lennon, B.A. and Pellegrino, S., Stability of Lobed Inflatable Structures, *41st AIAA/ASME/ASCE/AHS/ASC Structures, Structural Dynamics and Materials Conference and Exhibit*, Atlanta (GA), 3–6 April, 2000.

14. Lennon, B.A., Stiff Structure Analogies for Analysis of Lobed Inflatable Membrane Structures, *5th International Conference on Computation of Shell and Spatial Structures*, Ramm, E., Wall, W.A., and Bletzinger, K.-U., Bischoff, M. (eds.), Salzburg, 1–4 June, 2005.

15. Pagitz, M., Xu, Y. and Pellegrino, S., Buckling of Pumpkin Balloons, *5th International Conference on Computation of Shell and Spatial Structures*, Ramm, E., Wall, W.A., and Bletzinger, K.-U., Bischoff, M. (eds.), Salzburg, 1–4 June, 2005.